©2004 by Economic Geology
Vol. 99, pp. 1711–1725

Sulfur Isotope Evidence for Magmatic Contributions to Submarine and Subaerial Gold Mineralization: Conical Seamount and the Ladolam Gold Deposit, Papua New Guinea

J. Bruce Gemmell,† Robina Sharpe,

Centre for Ore Deposit Research (CODES SRC), University of Tasmania, Private Bag 79, Hobart, Tasmania, Australia 7001

Ian R. Jonasson,

Geological Survey of Canada, 601 Booth Street, Ottawa, Ontario, Canada K1A 0E8

and Peter M. Herzig

Institute for Mineralogy, Freiberg University of Mining and Technology, Brennhausgasse 14, D-09599, Freiberg, Germany

Abstract

Conical seamount is a submarine alkali basalt volcano situated 10 km south of Lihir Island in the Tabar-Feni island chain, Papua New Guinea. Polymetallic (Zn-Pb-Ag-Au-As-Sb) veins, pyritic stockwork, and hydrothermally altered rocks discovered on the summit of Conical seamount represent a unique example of submarine gold mineralization with mineralogical, chemical, and textural characteristics common to some subaerial epithermal systems. The giant Ladolam epithermal gold deposit (42 Moz Au) is situated in the crater of an alkali stratovolcano on Lihir Island. Portions of the epithermal mineralization and alteration assemblages at Ladolam are similar to those observed on Conical seamount.

Conical seamount has the lightest, hydrothermal (i.e., nondiagenetic) sulfide $\delta^{34}S$ values (–17.5 to +6.1‰) measured to date from modern sea-floor hydrothermal systems. A previous model for the Conical seamount hydrothermal system suggested a contribution of magmatic volatiles in the earliest stages of mineralization (stage 1), followed by a combination of sulfur leached from the underlying volcanic rocks and reduced seawater sulfate during the main base and precious metal precipitating event (stage 2). New sulfur isotope data allow a reinterpretation of this model that suggests a greater input of magmatic volatiles, plus boiling, throughout both stage 1 and 2 mineralization.

Sulfides from the Ladolam gold deposit have a range of sulfur isotope values (–12.9 to +3.6‰) similar to that of Conical seamount. These sulfur isotope data have previously been interpreted as the result of magmatic volatiles escaping from a crystallizing magma and mixing with dilute meteoric ground water. Anhydrite associated with the gold mineralization has two populations of $\delta^{34}S$ values (8–14 and 20–22‰), which indicate the interaction of magmatic volatiles with seawater that has previously been discounted. The range of sulfide and sulfate $\delta^{34}S$ values at Ladolam is reinterpreted to be due to a complex interaction of magmatic hydrothermal fluids, meteoric ground water, and seawater. Native sulfur in thermal areas in Luise caldera and pyrite in offshore hydrothermal vents in Luise harbor have similar $\delta^{34}S$ values to the Ladolam epithermal mineralization, indicating that fluids similar to the young Ladolam ore-forming event are still reaching the floor of Luise caldera.

Sulfur isotope data from Conical seamount and the Ladolam deposit suggest that magmatic volatiles have contributed a significant amount of sulfur to both these gold-rich hydrothermal systems.

Introduction

Magmatic contributions to the genesis of both active and extinct volcanic-hosted massive sulfide (VHMS) and epithermal deposits have been the subject of considerable debate (e.g., Hedenquist and Lowenstern, 1994). Sillitoe et al. (1996), Hannington (1997), and Hannington et al. (1999) recognized that the same characteristic geological and geochemical features that separate epithermal deposits into high- and low-sulfidation styles occur within the family of polymetallic (Cu-Pb-Zn-Ag-Au) sea-floor, volcanic-hosted massive sulfide deposits situated in submarine, arc tectonic environments. Resolving the role and significance of magmatic fluid is critical to the understanding the sources of sulfur and metals in the formation of mineral deposits in submarine settings (de Ronde, 1995; Herzig and Hannington, 1995a; Sillitoe et al., 1996; Yang and Scott, 1996; Herzig et al., 1998a; Gemmell et al., 1999; Hannington et al., 1999). This paper contributes data relevant to constraining the source(s) of sulfur in two gold-rich hydrothermal systems in the southwestern Pacific Ocean: the submarine Conical seamount system and the subaerial Ladolam gold deposit on Lihir Island, Papua New Guinea.

Petersen et al. (2002) published initial sulfur isotope data for Conical seamount, and two sulfur isotope studies on the Ladolam deposit have been published by Müller (2002a) and Carman (2003). We report new laser-ablation and conventional sulfur isotope data for Conical seamount, as well as new conventional sulfur isotope data for the Ladolam deposit, active hot spring deposits on Lihir Island, and pyritic hydrothermal vents in Luise harbor, offshore from Lihir Island. These data are used to refine interpretations of the sources of sulfur for both Conical seamount and the Ladolam hydrothermal systems.

† Corresponding author: e-mail, Bruce.Gemmell@utas.edu.au

Regional Setting

The Pliocene-Pleistocene Tabar-Feni island chain, which includes Lihir Island and Conical seamount, occurs in a complex tectonic zone at the eastern edge of the Bismarck Sea. These islands are located in the former Oligocene fore-arc region of New Ireland on a large uplifted block raised by regional southward compression along the Manus-Kilinailau trench (Fig. 1A), and the present volcanism throughout the island chain is most likely related to subduction from the south along the New Britain-Solomon trench (Exon et al., 1986; Stewart and Sandy, 1988; McInnes et al., 1999, 2001). The mafic to intermediate volcanic rocks occurring on the Tabar-Feni islands formed from a high K, alkaline, SiO_2-undersaturated magma (Kennedy et al., 1990; McInnes, 1992; McInnes et al., 1999). These highly oxidized, sulfur-rich alkaline melts are interpreted to be generated by partial remelting of metasomatically enriched Oligocene mantle wedge regions (McInnes and Cameron, 1994; McInnes et al., 1999, 2001) and are considered to have risen through the old fore-arc crust along reactivated transfer faults (Herzig et al., 1998b).

Conical Seamount

Conical seamount is a submarine volcano located 10 km south of Lihir Island in the Tabar-Feni island chain, eastern Papua New Guinea (Fig. 1B; Herzig et al., 1994; Herzig and Hannington, 1995b). Conical seamount consists of vesicular, coherent, and brecciated pyroxene-phyric, alkali-olivine basalt and trachybasalt and is considered the first example of sea-floor hydrothermal activity associated with alkaline volcanism in an arc tectonic setting (Herzig et al., 1994; Herzig and Hannington, 1995b; Petersen et al., 2002).

A comprehensive sampling program, via TV-controlled grab and dredging, recovered more than 1,200 kg of mineralized material (Herzig et al., 1998c). Polymetallic (Zn-Pb-Ag-Au-As-Sb) veins, pyritic stockwork, and hydrothermally altered rocks discovered on the summit of Conical seamount provide an example of submarine gold-rich mineralization. There are a number of mineralogical, chemical, and textural characteristics in common with some subaerial epithermal systems (Herzig et al., 1998b, c; Petersen et al., 2002). Gold concentrations in samples from Conical seamount reach 230 ppm Au, with an average of 25 ppm (n = 40) and are the highest yet discovered on the present-day sea floor (Herzig et al., 1999; Petersen et al., 2002). Three stages of mineralization are observed at Conical seamount (Table 1), and these stages occur in three distinct zones: inner, intermediate, and outer (Fig. 2). All three mineralization stages occur in the inner zone, whereas the intermediate and outer zones both contain only stages 1 and 3. The main, gold-bearing stage 2 mineralization is confined to a relatively small area near the summit fissure. Examples of the Conical seamount mineralization stages analyzed in this study are shown in Figure 3.

Ladolam Deposit, Lihir Island

Lihir Island consists of several Pliocene to Pleistocene stratovolcanoes (Fig. 4A) composed mainly of alkali basalts, trachybasalts, and trachyandesites (Wallace et al., 1983; Kennedy et al., 1990; Moyle et al., 1990, Müller et al., 2001, 2002a, b). The youngest of these structures, the Luise volcano (0.35–0.9 Ma; Davies and Ballantyne, 1987), hosts the Ladolam Au deposit. Economic concentrations of gold occur in four main areas within the caldera (Lienetz, Minifie, Kapit, and Coastal zones). The total Au resource is 471 million tons (Mt) at 2.75 g/t Au for a total of 42 Moz Au (S. Hunt, pers. commun., 2001). Carman (1994, 2003) divided the mineralization at Ladolam into three stages: porphyry, transitional,

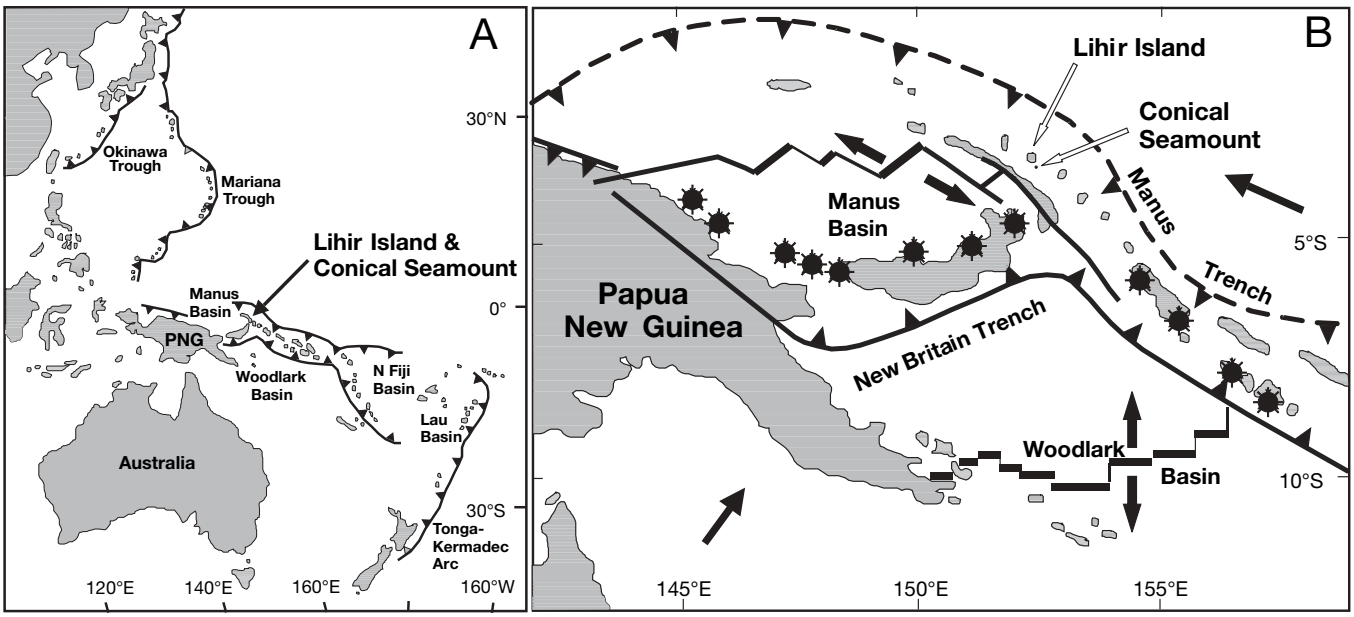

FIG. 1. A. Location of Lihir Island and Conical seamount in the southwest Pacific Ocean. Subduction trenches and important submarine hydrothermal sites of the western and southwestern Pacific Ocean are shown. B. Location of Lihir Island and Conical seamount in relationship to the tectonic features of eastern Papua New Guinea. Black starred circles are active volcanoes. Modified from Shipboard Scientific Party (2002).

TABLE 1. Characteristics of Mineralization at Conical Seamount and the Ladolam Deposit

	Stage	Style	Mineralogy	Alteration	Relationship to gold mineralization
Conical seamount[1]					
	1	Stockwork veins, veinlets, and disseminations	Pyrite ± marcasite	Illite/smectite, amorphous silica, ± chlorite, kaolinite, alunite, and rare aluminum phosphate sulfate minerals	Premineralization
	2	Veins and disseminations	Sphalerite, chalcopyrite, galena, pyrite, Cu-Pb-As-Sb sulfosalts, native gold, electrum	Amorphous silica-chalcedony, illite, smectite, adularia, secondary Na-K plagioclase, chlorite, kaolinite, barite, and rare apatite	Synmineralization
	3	Filling fractures, vesicles, and overgrowths	Realgar, alacranite, orpiment, stibnite, pyrite, amorphous silica	No obvious alteration	Postmineralization
Ladolam deposit[2]					
	I	Porphyry veinlets and disseminations	Chalcopyrite, molybdenite, pyrite	Biotite, orthoclase, albite, anhydrite, rutile, muscovite, magnetite, pyrite, ± tremolite, apatite, tourmaline, chlorite, calcite	Premineralization, related to porphyry-style mineralization
	II	Transitional epithermal veins and breccia matrix	Shallow: pyrite, ± marcasite, arsenopyrite Deep: pyrite ± sphalerite, galena, pyrrhotite, chalcopyrite, molybdenite	Shallow: adularia Deep: adularia, anhydrite, pyrite, vermiculite ± barite, calcite	Synmineralization
	III	Late epithermal veins	Pyrite, marcasite	Argillic/advanced argillic-kaolinite ± alunite, smectite Silicic quartz, mixed layer clay ± adularia, anhydrite, calcite	Postmineralization, postdates refractory ores, possible redistribution of gold

[1] Petersen et al. (2002)
[2] Carman (1994, 2003)

and epithermal (Table 1). The Ladolam hydrothermal system is still active, with thermal areas within Luise caldera (Fig. 4B) consisting of mud pools, boiling springs of chloride and acid sulfate fluids, and low-temperature fumaroles (Wallace et al., 1983; Moyle et al., 1990). At the shoreline, and extending up to 100 m offshore, active hydrothermal venting (Fig. 4B) has formed crusts of colloform-banded pyrite in volcaniclastic sand (Pichler et al., 1999).

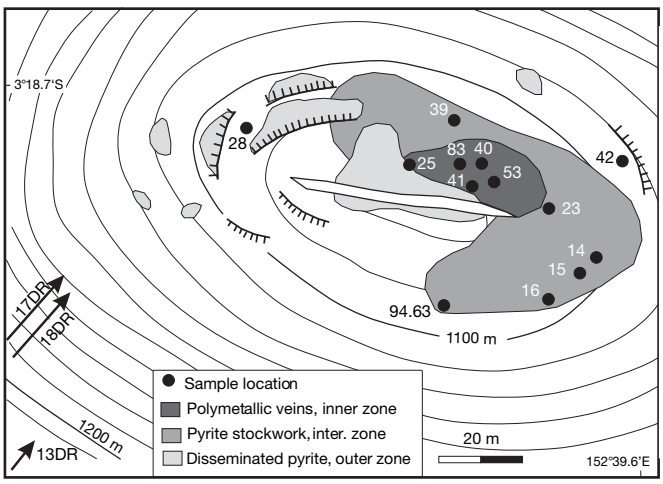

FIG. 2. Bathymetric map of the summit plateau region of Conical seamount, illustrating the different zones of mineralization and alteration. Hachured lines are scarps and open gash is an eruptive fissure (ridge) across top of the seamount. Sulfur isotope sample locations, from TV grab sampling, shown as black circles. Lines with arrows indicate dredge sample tracks and dredge direction. Modified from Petersen et al. (2002).

Sulfur Isotope Geochemistry

Methods

Although a minor amount of the sulfide from Conical seamount is coarse enough for separation by conventional methods, the very fine grained nature of the majority of the sulfides requires use of the laser-ablation technique to obtain $\delta^{34}S$ data. The laser-ablation technique also allows for detailed analysis of in situ mineral intergrowths and traverses across multigenerational veins. These types of detailed sulfur isotope analyses have not been reported previously for samples from Conical seamount. New $\delta^{34}S$ data for the Ladolam deposit, Luise caldera thermal areas, and Luise harbor offshore hydrothermal vents were obtained using conventional methods. Details of the analytical procedures are listed in Table 2.

Conical seamount

One hundred and two (43 conventional and 59 laser-ablation) sulfur isotope analyses of pyrite, sphalerite, and galena from stages 1 and 2 indicate $\delta^{34}S$ values ranging from –17.5 to

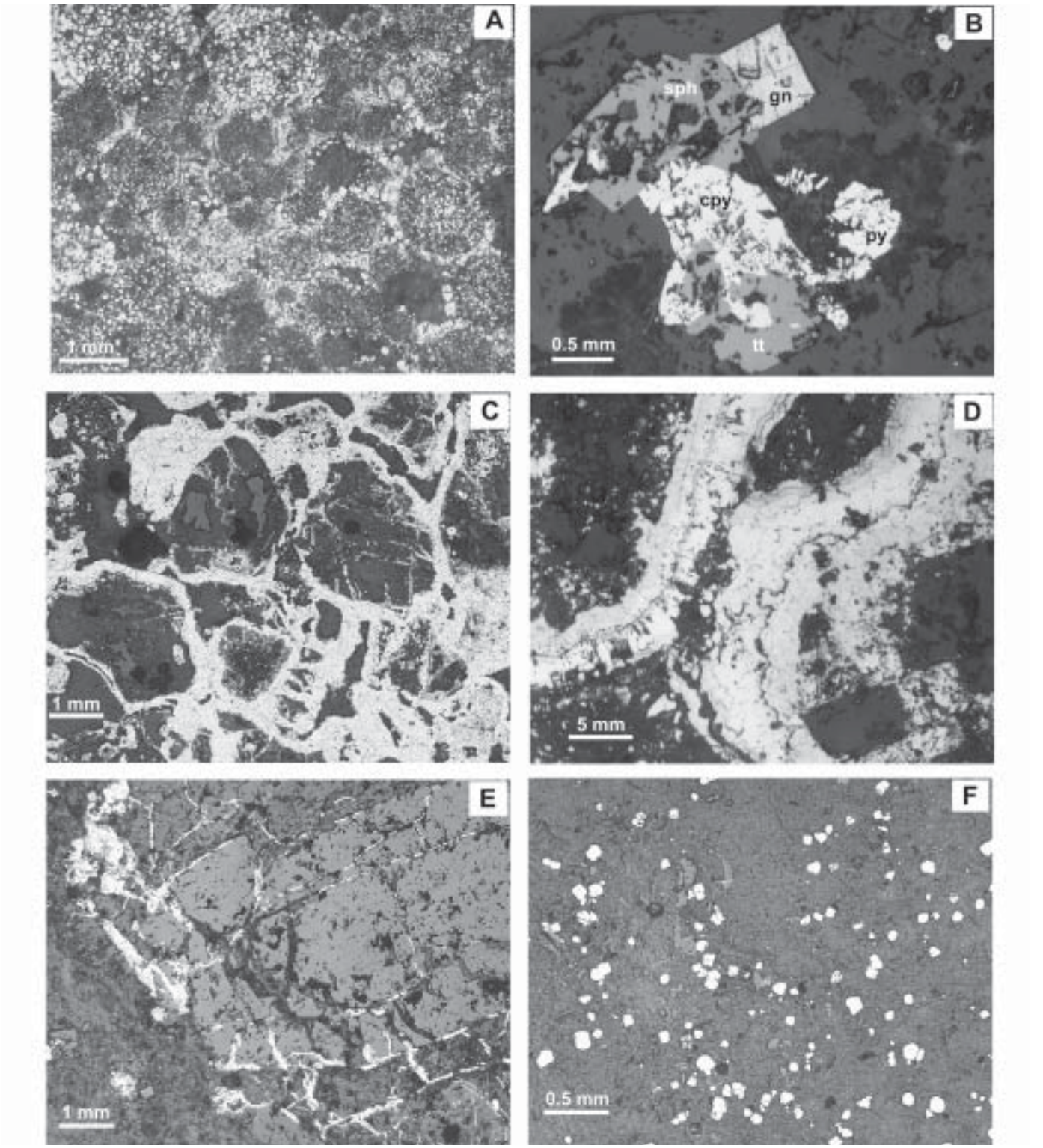

FIG. 3. Examples of Conical seamount mineralization stages analyzed in this study. A. Stage 1 pyrite-marcasite replacing magnetite, veinlets through altered clinopyroxene and magnetite, and scattered grains in basalt breccia (sample 25GTVA-4; inner zone). B. Stage 2 galena (gn), sphalerite (sph), chalcopyrite (cp), tetrahedrite-tennantite (tt) and pyrite (py) in silicified basalt (sample 25GTVA-5C; inner zone). C. Stage 1 pyrite-marcasite grains disseminated in basalt groundmass, lining vesicles, rimming and replacing pyroxene phenocrysts, and as colloform and crustiform veins in basalt breccia (sample 39GTVA-1D; intermediate zone). D. Stage 1 banded pyrite veins in silica-pyrite–altered basalt breccia (sample 39GTVA-2C; intermediate zone). E. Stage 1 pyrite filling fractures, rimming magnetite phenocrysts and occurring as disseminated grains in the groundmass of weakly altered basalt (sample 14GTVA-4A; outer zone). F. Stage 1 disseminated pyrite in weakly clay-altered basalt (sample 14GTVA-3; outer zone).

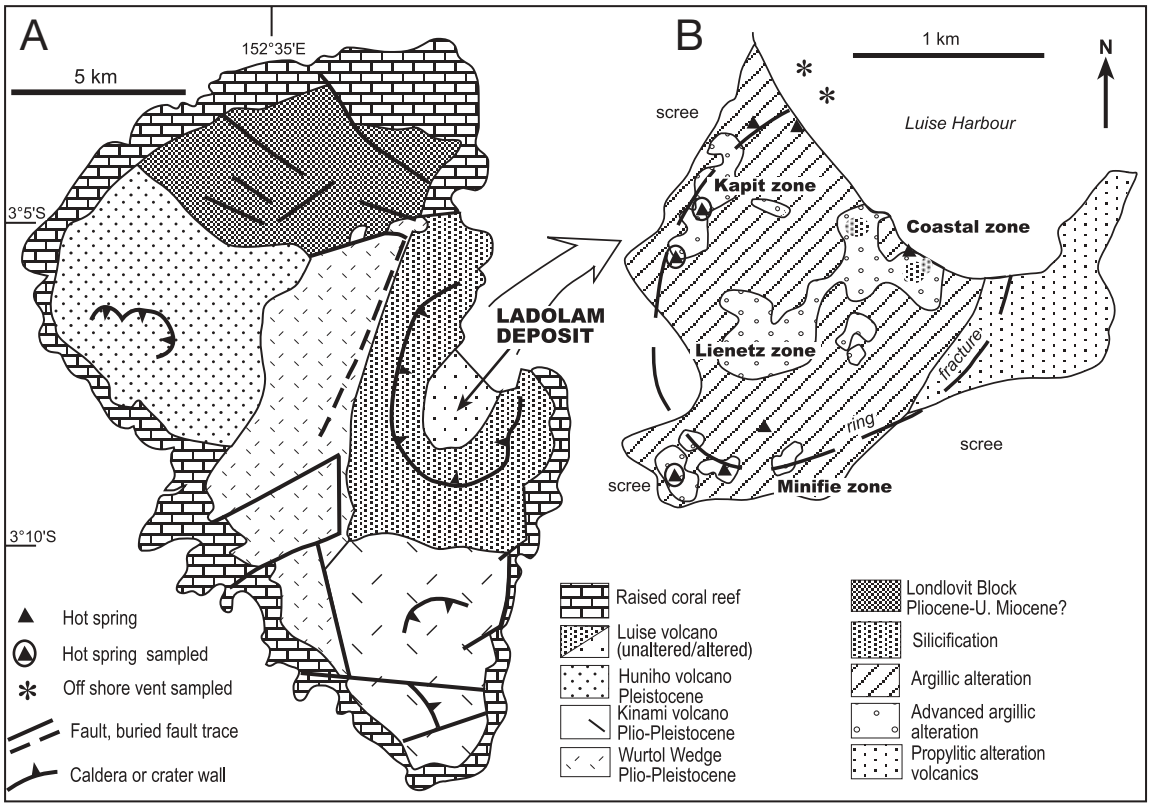

FIG. 4. A. Geology of Lihir Island. B. Location of alteration and mineralized zones of the Ladolam deposit and locations of fumaroles within the crater and offshore hydrothermal vents in the harbor. Modified from Moyle et al. (1990), Richards (1995) after Wallace et al. (1983), and Corbett and Leach (1998).

+6.1 per mil, with a mean of –1.9 per mil (Tables 2–3, Fig. 5A). Stage 1 pyrite varies from –17.5 to +6.1 per mil, with a mean of –1.6 per mil. The δ^{34}S values of stage 2 base metal sulfide vary over a smaller range of –9.5 to +3.9 per mil, with a mean of –2.1 per mil. Petersen et al. (2002) reported 28 sulfide and three sulfate δ^{34}S values from Conical seamount, indicating similar ranges (Table 3).

A comparison of sulfur isotope values between paragenetic stages through the inner, intermediate, and outer mineralized zones is given in Table 3 and Figure 5B. Sulfur isotope values for all sulfides from stages 1 and 2 in the inner zone vary from –13.9 to +6.0 per mil, with a mean of –1.2 per mil (Fig. 5C). Stage 2 sphalerite (–3.0 to +1.1‰; mean = –1.1‰) and galena (–9.5 to +3.9‰; mean = –4.4‰) lie within the range of stage 1 pyrite (–13.9 to +6.0‰; mean = –2.3‰). The inner zone appears to have two populations of δ^{34}S values (Fig. 5C); the majority of values range from –4 to +6 per mil, with a second population between –7 to –14 per mil. The group of lower δ^{34}S values data consists of pyrite and galena in altered basalt breccias, and the group of higher δ^{34}S values consists of pyrite, sphalerite, and galena in both altered basalt breccias and pyrite veins. Sulfur isotope values for stage 1 pyrite in the intermediate zone vary from –7.3 to +3.3 per mil, with a mean of –0.1 per mil (Fig. 5C). Sulfur isotope values for all stage 1 pyrite in the outer zone vary from –17.5 to +6.1 per mil, with a mean of –4.7 per mil (Fig. 5C).

Although the Conical seamount sulfides have a wide range of δ^{34}S values, these values vary systematically both in time and space. There is a paragenetic trend from the lowest δ^{34}S values in stage 1 pyrite, followed by stage 2 sphalerite and galena, with the late-stage arsenic minerals having the highest δ^{34}S values, as noted by Petersen et al. (2002). In conjunction with this shift to higher δ^{34}S values with successive paragenetic stages, there is a variation from higher δ^{34}S values in the inner and intermediate zones to progressively lower δ^{34}S values in the outer zone (Fig. 5C). The fractionation between sulfide pairs (Table 2) leads to unrealistic temperatures for sulfur isotope geothermometers and indicates that the sulfides did not precipitate in isotopic equilibrium.

Ladolam deposit, Lihir Island

New sulfide and sulfate δ^{34}S data for epithermal mineralization, anhydrite veins, sulfur deposited from fumaroles, and pyrite associated with offshore hydrothermal vents are given in Table 4. These data are compared to published δ^{34}S data by Müller et al. (2002a) and Carman (2003) in Figure 6A and Table 5.

Figure 6B compares sulfide and sulfate δ^{34}S values for the Ladolam deposit with the new data. The δ^{34}S analyses of epithermal mineralization determined in this study lie within the range of δ^{34}S values for epithermal mineralization as reported by Müller et al. (2002a) and Carman (2003). The

TABLE 2. Conical Seamount Sulfur Isotope Data

Sample no.	Description	Paragenetic stage	Mineral	$\delta^{34}S$ (‰)	Method[1]
Inner zone					
25 GTVA 4	Mineralized amorphous silica-altered basalt breccia-sulfide separate	2	Galena	–9.5	Conv.
25 GTVA 4	Mineralized amorphous silica-altered basalt breccia-sulfide separate	2	Sphalerite	–0.8	Conv.
25 GTVA-4	Euhedral pyrite in matrix of amorphous silica-altered basalt breccia	1	Pyrite	1.2	Laser
25 GTVA-4	Subhedral pyrite in matrix of amorphous silica-altered basalt breccia	1	Pyrite	1.2	Laser
25 GTVA-4	Euhedral pyrite in matrix of amorphous silica-altered basalt breccia	1	Pyrite	2.6	Laser
25 GTVA 5C	Mineralized amorphous silica-altered basalt breccia-sulfide separate	2	Sphalerite	–3.0	Conv.
25 GTVA-5C	Pyrite in Fe oxide-realgar-amorphous silica basalt breccia matrix	1	Pyrite	1.2	Laser
25 GTVA-5C	Pyrite in Fe oxide-realgar-amorphous silica basalt breccia matrix	1	Pyrite	2.0	Laser
25 GTVA-5C	Anhdreal pyrite in matrix of amorphous silica-altered basalt breccia	1	Pyrite	1.8	Laser
25 GTVA-6A(i)	Sulfide vein in amorphous silica-altered basalt breccia	2	Sphalerite	–1.2	Conv.
25 GTVA-6A(ii)	Sulfide vein in amorphous silica-altered basalt breccia	2	Pyrite	–2.4	Conv.
25 GTVA-6B	Mineralized amorphous silica-altered basalt breccia	2	Pyrite	0.9	Conv.
25 GTVA 6B1	Mineralized amorphous silica-altered basalt breccia	2	Sphalerite	1.1	Conv.
25 GTVA-8	Pyrite replacing clast in amorphous silica-altered basalt breccia	1	Pyrite	2.1	Laser
25 GTVA-8A	Anhedral pyrite in matrix of amorphous silica-altered basalt breccia	1	Pyrite	1.9	Laser
25 GTVA-8A	Anhedral pyrite in matrix of amorphous silica-altered basalt breccia	1	Pyrite	1.8	Laser
25 GTVA 8C	Semimassive sulfide in amorphous silica altered basalt breccia	2	Galena	–0.8	Conv.
25 GTVA 8C2	Semimassive sulfide in amorphous silica altered basalt breccia	2	Sphalerite	0.8	Conv.
40-GTVA-1	Altered basalt-sulfide concentrate	1	Pyrite	–2.6	Conv.
40 GTVA-1B	Disseminated pyrite in altered basalt	1	Pyrite	–7.5	Conv.
40 GTVA-2	Clay-pyrite altered basalt-sulfide separate	1	Pyrite	–0.4	Conv.
40 GTVA-2	Clay-pyrite altered basalt-sulfide separate	1	Pyrite	–0.4	Conv.
40 GTVA-2	Euhedral pyrite in matrix of clay-amorphous silica altered basalt	1	Pyrite	4.0	Laser
40 GTVA-2	Euhedral pyrite in matrix of clay-amorphous silica altered basalt	1	Pyrite	3.1	Laser
40 GTVA-2.2	Pyrite vein in clay-amorphous silica altered basalt	1	Pyrite	6.0	Laser
40 GTVA-2.2	Pyrite vein in clay-amorphous silica altered basalt	1	Pyrite	4.6	Laser
41 GTVA-1A	Euhedral pyrite in altered feldspar	1	Pyrite	2.6	Laser
41 GTVA-1A	Subeuhedral pyrite in clay-amorphous silica-altered basalt	1	Pyrite	4.8	Laser
53 GTVA 1B	Sulfide-amorphous silica alteration of basalt-sulfide separate	1	Pyrite	–13.7	Conv.
53 GTVA-1A	Sulfide-amorphous silica alteration of basalt-sulfide separate	1	Pyrite	–11.5	Conv.
53 GVTA-1A	Subhedral pyrite in sulfide-amorphous silica alteration of basalt	1	Pyrite	–13.4	Laser
53 GVTA-1A	Spongy pyrite in sulfide-amorphous silica alteration of basalt	1	Pyrite	–9.4	Laser
53 GVTA-1A	Finely banded pyrite rim of cavity in basalt	1	Pyrite	–11.6	Laser
53-GTVA-1A	Sulfide-amorphous silica alteration of basalt-sulfide separate	1	Pyrite	–13.9	Conv.
53-GTVA-1A2	Sulfide-amorphous silica alteration of basalt-sulfide separate	1	Pyrite	–13.0	Conv.
53 GTVA 2A	Amorphous silica-chlorite alteration of basalt-sulfide separate	2	Galena	–2.5	Conv.
53 GTVA 2A	Amorphous silica-chlorite alteration of basalt-sulfide separate	2	Sphalerite	–3.0	Conv.
53 GTVA-2A	Pyrite in amorphous silica-chlorite alteration of basalt breccia	1	Pyrite	1.5	Laser
53 GTVA-2A	Spongy pyrite in amorphous silica-chlorite alteration of basalt breccia	1	Pyrite	3.6	Laser
53 GTVA-2A	Spongy pyrite in amorphous silica-chlorite alteration of basalt breccia	1	Pyrite	4.3	Laser
53 GTVA-2A	Galena in amorphous silica-chlorite alteration of basalt breccia	2	Galena	3.9	Laser
53 GTVA 2B	Amorphous silica-chlorite alteration of basalt-sulfide separate	1	Pyrite	–9.6	Conv.
53 GTVA 3A	Sulfide-sulfosalt veins in amorphous silica matrix-sulfide separate	2	Galena	–2.5	Conv.
53 GTVA 3A	Sulfide-sulfosalt veins in amorphous silica matrix-sulfide separate	2	Sphalerite	–1.7	Conv.
83 GTVA 2A1	Disseminated pyrite in amorphous silica-altered basalt-sulfide separate	1	Pyrite	–1.7	Conv.
83 GTVA-2B2	Subeuhedral pyrite in amorphous silica-altered basalt	1	Pyrite	5.7	Laser
83 GTVA-2C1	Pyrite veinlets in amorphous silica-altered basalt-sulfide separate	1	Pyrite	2.9	Laser
83 GTVA-2C1	Subhedral disseminated pyrite in amorphous silica-altered basalt	1	Pyrite	0.0	Laser
83 GTVA-2C1	Eu- and/or subhedral pyrite lining vesicle in amorphous silica-altered basalt	1	Pyrite	0.6	Laser
83 GTVA 2C1	Pyrite veinlet in amorphous silica-altered basalt-sulfide separate	1	Pyrite	–2.7	Conv.
Intermediate zone					
23 GTVA 1	Pyrite in amorphous silica-altered basalt breccia-sulfide separate	1	Pyrite	–7.3	Conv.
23 GTVA-1	Pyritic mud	1	Pyrite	–5.6	Conv.
23 GTVA-5	Rim of pyrite band, amorphous silica-altered basalt breccia	1	Pyrite	–0.5	Laser
23 GTVA-5	Center of pyrite band, amorphous silica-altered basalt breccia	1	Pyrite	–1.6	Laser
23 GTVA-5	Disseminated pyrite in amorphous silica-altered basalt breccia	1	Pyrite	–3.9	Laser
23 GTVA-5	Spongy pyrite in matrix of amorphous silica-altered basalt breccia	1	Pyrite	–4.4	Laser
23 GTVA-5	Anhedral pyrite in matrix of amorphous silica-altered basalt breccia	1	Pyrite	–4.4	Laser
39 GTVA 1X	Massive colloform sulfide-sulfide separate	1	Pyrite	–3.9	Conv.
39 GTVA-1A	Pyrite-sulfide rock with native S on surface	1	Pyrite	–0.1	Conv.
39 GTVA-1C	Pyrite-sulfide rock with native S on surface	1	Pyrite	0.9	Conv.
39 GTVA-1D	Colloform banded pyrite	1	Pyrite	2.6	Laser
39 GTVA-1D	Anhedral pyrite in semimassive pyrite	1	Pyrite	1.6	Laser
39 GTVA-1D	Massive aggregate pyrite in semimassive pyrite	1	Pyrite	2.4	Laser
39 GTVA-1D	Spongy, anhedral pyrite in semimassive pyrite	1	Pyrite	1.3	Laser

TABLE 2. *(Cont.)*

Sample no.	Description	Paragenetic stage	Mineral	$\delta^{34}S$ (‰)	Method[1]
39 GTVA-1E	Pyrite rim around amorphous silica-altered basalt breccia clast	1	Pyrite	2.3	Laser
39 GTVA-1E	Pyrite matrix of altered basalt breccia	1	Pyrite	1.8	Laser
39 GTVA-1E	Radial zoned pyrite replacement of basalt clast	1	Pyrite	0.9	Laser
39 GTVA-1E	Euhedral pyrite lining cavity in altered basalt breccia	1	Pyrite	1.2	Laser
39 GTVA-2A	Spongy pyrite in center of crustiform pyrite vein	1	Pyrite	1.1	Laser
39 GTVA-2A	Massive pyrite in middle of pyrite vein	1	Pyrite	3.3	Laser
39 GTVA-2A	Spongy pyrite from margin of pyrite vein	1	Pyrite	1.7	Laser
39 GTVA-2A	Pyrite veins in weakly altered basalt-sulfide separate	1	Pyrite	–2.1	Conv.
39 GTVA-2C	Pyrite at wall rock-vein margin	1	Pyrite	1.9	Laser
39 GTVA-2C	Band of spongy pyrite toward middle of vein	1	Pyrite	0.8	Laser
39 GTVA-2C	Radial and/or spherical spongy pyrite from middle of vein	1	Pyrite	–1.5	Laser
39 GTVA-2C	Band of pyrite in middle of vein	1	Pyrite	0.7	Laser
39 GTVA-2C	Band of radial pyrite near outer vein margin	1	Pyrite	0.3	Laser
39 GTVA-2C	Subhedral pyrite grains at outer vein rim	1	Pyrite	–1.1	Laser
39 GTVA-2C	Subhedral pyrite in weakly altered basalt	1	Pyrite	1.9	Laser
39 GTVA-2C	Pyrite vein in weakly altered basalt-sulfide separate	1	Pyrite	0.4	Conv.
39 GTVA-2D	Pyrite vein in weakly altered basalt-sulfide separate	1	Pyrite	–1.1	Conv.
39 GTVA-2E	Pyrite vein in weakly altered basalt-sulfide separate	1	Pyrite	–0.4	Conv.
39 GTVA-2H	Pyrite vein in weakly altered basalt-sulfide separate	1	Pyrite	–0.3	Conv.
39 GTVA-3C	Pyrite alteration on outer surface of basalt-sulfide separate	1	Pyrite	0.5	Conv.
39-GTVA-2C	Pyrite veins in weakly altered basalt-sulfide separate	1	Pyrite	–0.2	Conv.
			Pyrite		
Outer zone			Pyrite		
13 DR-8C	Anhedral pyrite in weakly clay-altered basalt	1	Pyrite	4.6	Laser
14 GTVA 2X1	Pyrite in vesicles in basalt-sulfide separate	1	Pyrite	–3.8	Conv.
14 GTVA 2Y1	Pyrite in vesicles in basalt-sulfide separate	1	Pyrite	–5.0	Conv.
14 GTVA-3	Anhedral pyrite in weakly clay-altered basalt	1	Pyrite	–6.2	Conv.
14 GTVA-3	Euhedral pyrite in weakly clay-altered basalt	1	Pyrite	–1.5	Laser
14 GTVA-3	Massive pyrite at centre of pyrite vein	1	Pyrite	–3.1	Laser
14 GTVA-3	Spongy pyrite at margin of pyrite vein	1	Pyrite	–6.9	Laser
14 GTVA-3	Spongy pyrite at margin of pyrite vein	1	Pyrite	–2.4	Laser
14 GTVA-3	Massive well-formed pyrite in middle of vein	1	Pyrite	–4.6	Laser
14 GTVA-3	Spongy pyrite grain at rim of pyrite vein	1	Pyrite	–8.8	Laser
14 GTVA-4A	Pyrite rim to weakly altered clast in basalt breccia	1	Pyrite	–15.6	Laser
15 GTVA 2D	Pyrite in weak clay-amorphous silica altered basalt-sulfide separate	1	Pyrite	–17.5	Conv.
28-GTVA-2	Pyrite in weak amorphous silica altered basalt-sulfide separate	1	Pyrite	–11.6	Conv.
42 GTVA-2-2	Subhedral pyrite in oxidized margin of unaltered basalt	1	Pyrite	5.3	Laser
42 GTVA-2-2	Spongy pyrite within oxidized basalt	1	Pyrite	6.1	Laser
Conical 1	Pyrite concentrate, location unknown	1	Pyrite	–5.2	Conv.
Conical 2	Pyrite concentrate, location unknown	1	Pyrite	–5.2	Conv.

Abbreviations: Conv. = conventional sulfur isotope analysis, Dr = dredge sample, GTVA = TV grab sample

Paragenetic stage: 1 = early disseminated, vein, and semimassive pyrite, 2 = pyrite and polymetallic sulfides, and sulfosalts with gold mineralization

[1]For conventional sulfur isotope analyses, sulfides were handpicked or drilled out with the aid of a small-diameter dental drill; petrographic examination aided selection of sample sites that were monomineralic; the drill was cleaned between each sample extraction to ensure no cross-sample contamination; conventional sulfide separates were combusted with excess Cu_2O to produce SO_2, according to the methodology of Robinson and Kusakabe (1975); microanalytical determinations of sulfur isotopes used the Nd:YAG laser-ablation instrument at the Central Science Laboratory, University of Tasmania; operational procedures are reported in Huston et al. (1995); sulfur isotope ratios for both the conventional and laser-ablation methods were measured using a VG Isogas Sira II mass spectrometer located at the University of Tasmania; results are reported in standard notation relative to the Canon Diablo Troilite standard (CDT); sulfide standards (Rosebery 12.4‰ and Broken Hill 3.4‰) and a reference SO_2 gas were analyzed each day with the conventional or laser analyses to verify analytical procedures and quality of results; sample reproducibility is typically ±0.5 per mil; precision (1σ) of laser-ablation sulfur isotope analyses is 0.3 to 0.5 per mil compared to a precision of 0.1 to 0.3 per mil for conventional analyses at the University of Tasmania stable isotope facility (Huston et al., 1995)

fumarolic native sulfur and pyrite in offshore vents have the same $\delta^{34}S$ values as the Ladolam mineralization. New analyses of anhydrite show a greater range of $\delta^{34}S$ values (8.4–21.4‰) than previously reported (8.6–13‰, Table 5), indicating that anhydrite has two distinct populations of $\delta^{34}S$ values, one between 8 and 14 per mil and one between 20 and 22 per mil, although the possibility that there is a continuous range of $\delta^{34}S$ values cannot be ruled out, given the small number of samples analyzed.

Comparison between Conical seamount and the Ladolam deposit

Conical seamount and the Ladolam deposit have a similar range of sulfide $\delta^{34}S$ values (Fig. 7). Sulfides in the porphyry and transitional mineralization at Ladolam have $\delta^{34}S$ values consistent with those of stage 1 and 2 mineralization in the inner and intermediate zones at Conical seamount (Fig. 7). The epithermal mineralization at Ladolam has lower $\delta^{34}S$

TABLE 3. Summary of Conical Seamount Sulfur Isotope Data

		Mineral and analytical method	*n*	Mean (‰)	Minimum (‰)	Maximum (‰)
This study						
	Overall	All sulfides	102	–1.9	–17.5	6.1
		Conventional	43	–5.2	–17.5	1.1
		Laser	59	0.2	–15.6	6.1
	Stage 1	Pyrite	88	–1.6	–17.5	6.1
		Pyrite - conventional	30	–5.0	–17.5	0.9
		Pyrite - laser	58	0.1	–15.6	6.1
	Stage 2	Pyrite - conventional	2	0.8	–2.4	0.9
		Galena	4	–2.2	–9.5	3.9
		Galena - conventional	3	–4.3	–9.5	–0.8
		Galena - laser	1	3.9		
		Sphalerite - conventional	7	–1.1	–3.0	1.1
Petersen et al. (2002)[1]						
	Stage 1	Pyrite	15	–3.6	–8.6	–0.2
		Alunite	2	6.9	6.4	7.5
	Stage 2	Sphalerite-galena	7	0.6	–0.8	1.5
	Stage 3	Arsenic minerals	2	1.9	1.7	2.0
	Framboidal	Pyrite	3	–12.8	–13.9	–11.6

Abbreviations: *n* = number of analyses, arsenic minerals = realgar and alacranite
[1] All Petersen et al. (2002) samples analyzed by conventional method

TABLE 4. Ladolam Deposit, Luise Caldera, and Luise Harbor Sulfur Isotope Data

Sample	Location	Description	Mineral	$\delta^{34}S$ (‰)	Source[1]
Lihir 1	Lienetz	Stage III epithermal ore	Pyrite	–8.1	1
Lihir 1	Lienetz	Stage III epithermal ore	Pyrite	–10.0	1
Lihir 2	Lienetz	Stage III epithermal ore	Pyrite	–9.2	1
Lihir 4	Minifie	Stage III epithermal ore	Pyrite	–10.4	1
Lihir 4	Minifie	Stage III epithermal ore	Pyrite	–5.2	1
Lihir 5	Minifie	Stage III epithermal ore	Pyrite	–4.2	1
Lihir 6	Minifie	Stage III epithermal ore	Pyrite	–1.6	1
Lihir 6	Minifie	Stage III epithermal ore	Pyrite	–1.6	1
DDHL42-419	Lienetz	Anhydrite zone	Anhydrite	20.7	2
DDHL42-428	Lienetz	Anhydrite zone	Anhydrite	10.4	2
DDHL42-458	Lienetz	Anhydrite zone	Anhydrite	8.4	2
DDHL42-464	Lienetz	Anhydrite zone	Anhydrite-carbonate	12.5	2
DDHL44-321	Lienetz	Anhydrite zone	Anhydrite-carbonate	11.4	2
DDHL51-305	Lienetz	Anhydrite zone	Anhydrite	10.6	2
DDHL58-394	Lienetz	Anhydrite zone	Anhydrite	9.5	2
DDHL97-225	Minifie	Anhydrite zone	Anhydrite	10.5	2
DDHL122-210	Minifie	Anhydrite zone	Anhydrite	21.4	2
DDHL129-208	Minifie	Anhydrite zone	Anhydrite-carbonate	11.9	2
Minifie	Minifie	Fumarole	Native sulfur	–7.3	2
UK-1	Upper Kapit	Fumarole	Native sulfur	–7.2	2
UK-3(ii)	Upper Kapit	Fumarole	Native sulfur + clay	–5.0	2
LH-1	Luise harbor	Offshore vents	Pyrite-marcasite	–7.6	2
LH-3A	Luise harbor	Offshore vents	Pyrite-marcasite	–6.7	2
LH-3B	Luise harbor	Offshore vents	Pyrite-marcasite	–7.5	2
LH-7	Luise harbor	Offshore vents	Pyrite-marcasite	–7.9	2

All analyses by conventional sulfur isotope method
[1] Source: 1 = this study, 2 = M. Hannington, unpublished data

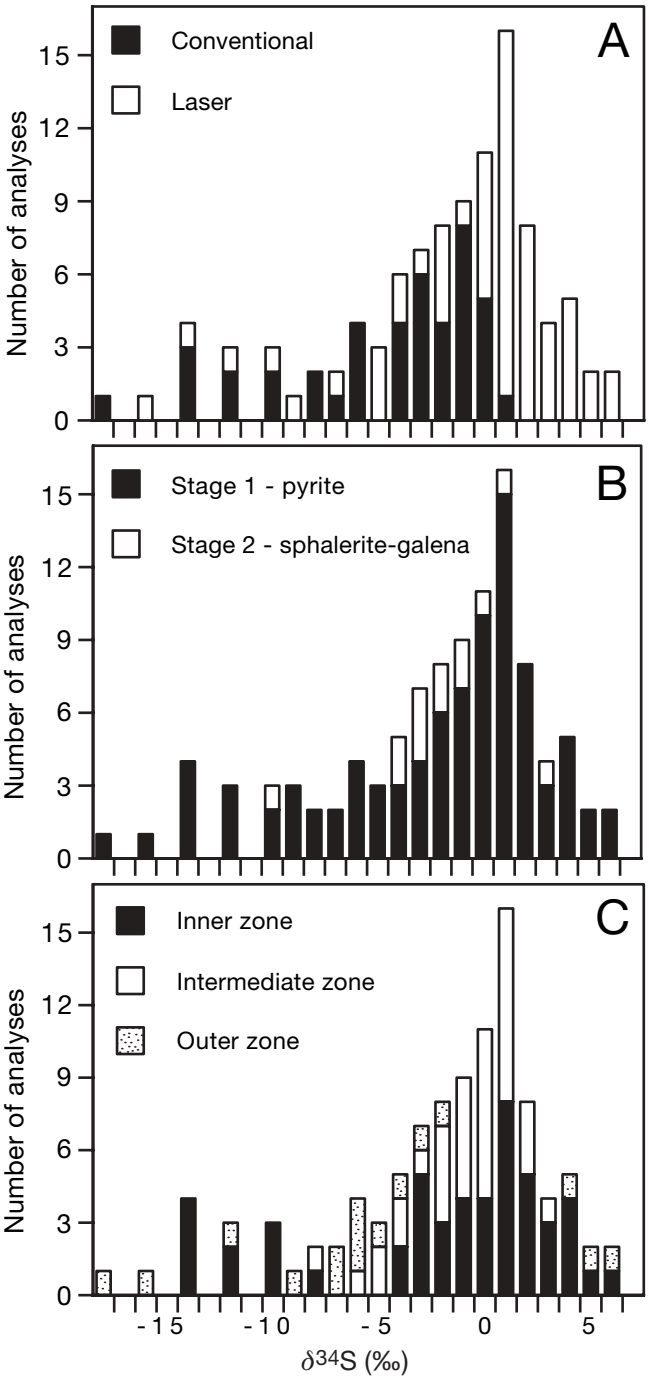

FIG. 5. Histograms of sulfide $\delta^{34}S$ analyses generated in this study for Conical seamount. A. Comparison of conventional vs. laser-ablation sulfide $\delta^{34}S$ values. B. Distribution of $\delta^{34}S$ values based on paragenetic stages. C. Distribution of $\delta^{34}S$ values based on mineralized zones. Data from Table 2.

values than the porphyry and transitional mineralization but similar values to the stage 1 mineralization in the outer zone at Conical seamount.

Comparison with other sea-floor hydrothermal systems

Sulfur isotope data for sulfide minerals and native sulfur from modern sea-floor hydrothermal sites have a wide range of values (Fig. 8). The $\delta^{34}S$ values for sulfides for unsedimented midocean ridges range from approximately –1 to +11 per mil, whereas the range for sedimented midocean ridges is –4 to +17 per mil. For midocean ridge hydrothermal systems, Shanks et al. (1995) concluded that the $\delta^{34}S$ values of vent fluid H_2S indicate that midocean ridge basalt (MORB) sulfur is the principal sulfur source, with a small contribution from inorganically reduced seawater sulfate. For hydrothermal systems in the sedimented-ridge environment the sources of sulfur include MORB, inorganic reduction of seawater sulfate, and a minor component of organically reduced seawater sulfate (Goodfellow and Franklin, 1993; Shanks et al., 1995; Goodfellow et al., 1999).

Sulfides from sea-floor hydrothermal systems forming in arc environments of the western Pacific (Fig. 1A) have $\delta^{34}S$ values that range from –8 to +16 per mil (Fig. 8). A comparison of the data in Figure 8 shows that the sulfur in sulfide minerals at Conical seamount is the lightest yet recorded for hydrothermal systems on the sea floor.

De Ronde (1995) concluded that active sea-floor systems located within back- or island arc environments may provide a link between the processes common to midocean ridge hydrothermal systems and those in subaerial settings, in terms of magmatic contributions to the hydrothermal fluid. Herzig et al. (1998c) suggested that the light sulfur in sulfides ($\delta^{34}S$ = –7.3 to –2.8‰, n = 12) and native sulfur ($\delta^{34}S$ = –4.8 to –2.4‰, n = 3) from the Hine Hina site in the Lau basin implied an ^{34}S-depleted source of probable magmatic origin. Samples from the DESMOS caldera, in the eastern Manus basin, have $\delta^{34}S$ values of –7 to –6 per mil (n = 6) for native sulfur forming in association with an advance argillic alteration. These $\delta^{34}S$ values are interpreted to be of magmatic derivation (Gamo et al., 1997; Gemmell et al., 1999). Samples from the PACMANUS site, also in the eastern Manus basin, have $\delta^{34}S$ values of –3 to +8 per mil (n = 85) for sulfides and 2 per mil for native sulfur that are interpreted to indicate a magmatic component in the hydrothermal fluid (Gemmell et al. 1996; J. B. Gemmell. unpub. data). Samples from another hydrothermal site in the eastern Manus basin, SuSu Knoll, have $\delta^{34}S$ values of sulfides –3 to 0 per mil (n = 13) for sulfides and –7 to +2 per mil (n = 13) for native sulfur that are interpreted to be magmatic (J. B. Gemmell, unpub. data). Samples from the Brothers volcano in the southern Kermadec arc have $\delta^{34}S$ values of –4 to +3 per mil for sulfides and –8 to –6 per mil for native sulfur, which de Ronde et al. (2000) suggested may indicate a magmatic sulfur component.

Comparison to epithermal deposits

Sulfides from low-sulfidation epithermal deposits (Fig. 9) have $\delta^{34}S$ values between –6 and +5 per mil, with the majority close to 0 per mil (Ohmoto and Rye, 1979, Field and Fifarek, 1985). Cooke and Simmons (2000) concluded that the waters that precipitate low-sulfidation epithermal mineralization have a magmatic volatile source for sulfur. Alkalic epithermal deposits have sulfide $\delta^{34}S$ values that vary from –7.9 to +5.5 per mil in the early magmatic-hydrothermal system, to –15 to +8 per mil (typically <0‰) in the epithermal system (Richards, 1995). Stable isotope compositions indicate a high proportion of magmatic fluids in most alkalic epithermal systems (Jensen and Barton, 2000). Sulfides from high-sulfidation epithermal deposits have $\delta^{34}S$ values that vary from –10 to +8 per mil

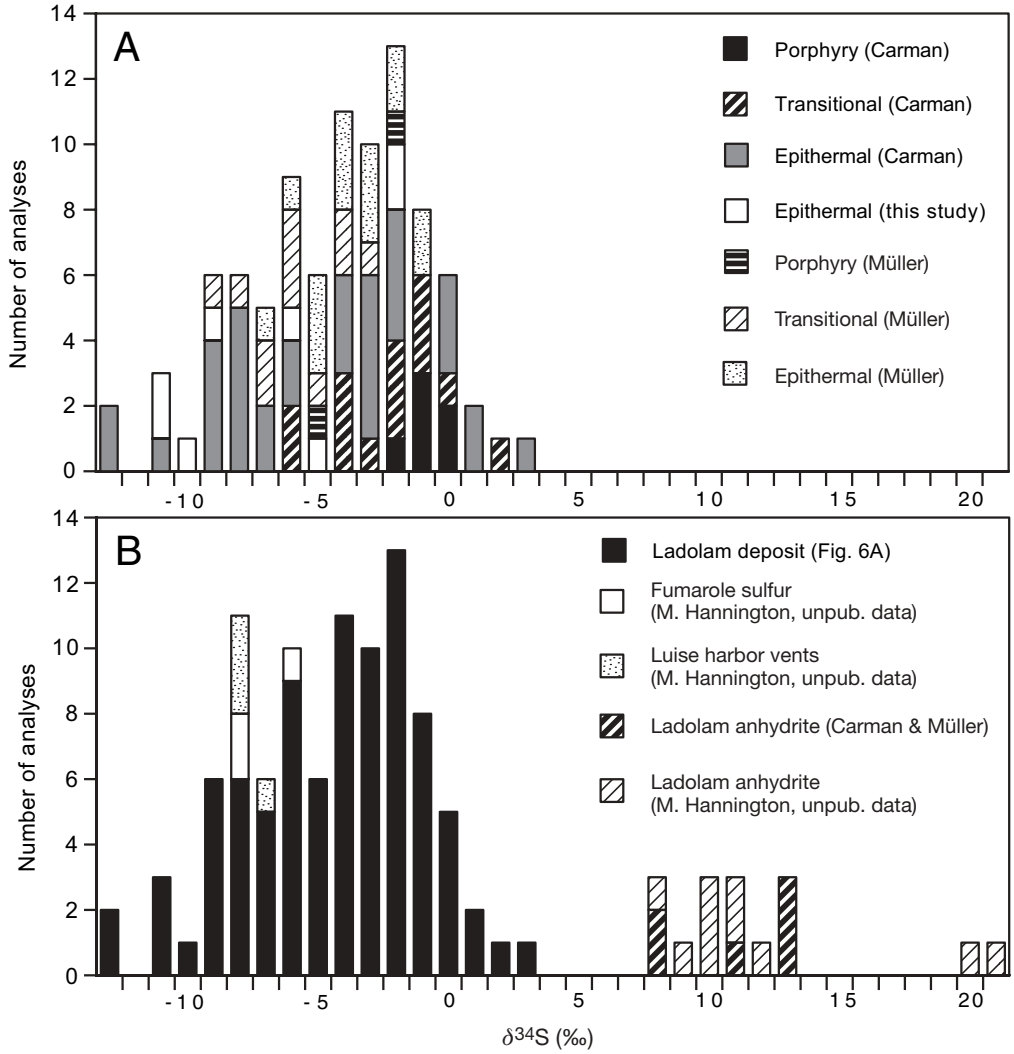

FIG. 6. Histograms of sulfide and sulfate $\delta^{34}S$ analyses for the Ladolam deposit. A. All sulfide $\delta^{34}S$ values for the different mineralization styles at the Ladolam deposit. B. $\delta^{34}S$ values for sulfides and anhydrite from the Ladolam deposit as well as native sulfur from thermal areas in Luise caldera and pyrite from offshore hydrothermal vents in Luise harbor. Data from Table 4, Müller et al. (2002a), and Carman (2003).

(Arribas, 1995), with the source of sulfur generally interpreted to be magmatic (Cooke and Simmons, 2000). Although sulfur isotope data for sulfides from Conical seamount and the Ladolam deposit overlap the data from all the different types of epithermal deposit, they are most similar to the epithermal portion of the alkalic-type epithermal deposits, inasmuch as they extend to unusually low $\delta^{34}S$ values.

Discussion

Comparison of analytical methods

A summary of the sulfur isotope data for Conical seamount (Table 3) illustrates that the conventional analyses tend to have a slightly narrower range (–17.5 to +1.1‰; mean = –5.2‰) compared to the laser-ablation analyses (–15.6 to +6.1‰; mean = 0.2‰). Although there appears to be a bias toward positive values obtained by the laser-ablation method compared to the conventional method (Table 3, Fig. 5A), close examination of the data suggests that this is not a consistent relationship throughout the sample suite. For example, pyrite from clay-pyrite alteration of basalt (sample 39GTVA-2C, Table 2) was analyzed both by laser-ablation and conventional methods with very similar results. The laser-ablation $\delta^{34}S$ values were –1.5 to +1.9 per mil (n = 7, mean = 0.4‰), whereas a pyrite separate analyzed by the conventional method has a $\delta^{34}S$ value of 0.4 per mil. Pyrite from pervasive amorphous silica-pyrite alteration of basalt (sample 53GTVA-1A, Table 2) has laser-ablation $\delta^{34}S$ values of –9.4, –11.6, and –13.4 per mil (mean = –12.8‰), and similar values of –11.5, –13.0, and –13.9 per mil (mean = –11.5‰) were obtained by the conventional method. Stringent analytical procedures (daily calibration using international sulfur isotope standards) adhered to in this study indicate that differences between the laser and conventional $\delta^{34}S$ analyses are due to sulfur isotope heterogeneity in the sulfides at Conical seamount, not a bias in the analytical method.

TABLE 5. Summary of Ladolam Deposit, Luise Caldera, and Luise Harbor Sulfur Isotope Data

		Mineral	*n*	Mean (‰)	Minimum (‰)	Maximum (‰)
This study[1]						
	Ladolam deposit	Stage III epithermal-pyrite	8	–6.3	–10.4	–1.6
		Anhydrite	10	12.7	8.4	21.4
	Kapit fumaroles	Native sulfur	3	–6.5	–7.5	–5.0
	Luise harbor vents	Pyrite-marcasite	4	–7.4	–7.9	–6.7
Carman (2003)[2]						
	Ladolam deposit	Stage I porphyry-pyrite	6	–0.4	–1.4	0.2
		Stage II transitional-pyrite, pyrrhotite	14	–2.0	–5.3	2.2
		Stage III epithermal-pyrite, marcasite, pyrrhotite, chalcopyrite	58	–4.3	–12.9	3.6
		Anhydrite	3	13	13	13
Müller et al. (2002a)[3]						
	Ladolam deposit	Stage I porphyry-pyrite	2	–3.2	–4.8	–1.6
		Stage II transitional-pyrite	11	–5.3	–8.8	–3.4
		Stage III epithermal-pyrite	15	–2.9	–6.0	–0.1
		Anhydrite	3	9.4	8.6	11.1

Abbreviations: *n* = number of analyses

[1] Ladolam deposit pyrite data from this study, analyzed by conventional method; Ladolam anhydrite, Kapit fumarole, and Luise harbour vent data from M. Hannington (unpub. data), analyzed by conventional method

[2] Carman (2003) samples analyzed by laser ablation and SHRIMP methods

[3] All Müller et al. (2002a) samples analyzed by conventional method

Conical seamount

Previous studies have suggested that sources of sulfur in sea-floor hydrothermal systems are direct magmatic emanations, inorganic reduction of seawater sulfate, leached magmatic sulfide, leached sulfate minerals followed by partial reduction, and a minor component of organically reduced seawater sulfate (Sangster, 1968; Ohmoto and Rye, 1979; Shanks et al., 1981; Ohmoto, 1986; Taylor, 1987; Solomon et al., 1988; Goodfellow and Franklin, 1993; Shanks et al., 1995; Goodfellow et al., 1999). Petersen et al. (2002) proposed a model for the evolution of the Conical seamount hydrothermal system where the very low δ^{34}S values for early framboidal pyrite and marcasite possibly indicates the influence of bacteriogenic sulfate reduction. They concluded that the platy habit of the alunite, the presence of aluminum phosphate sulfate minerals, and δ^{34}S values of coexisting pyrite and alunite are consistent with a contribution of magmatic volatiles in the earliest stages (i.e., stage 1) of the hydrothermal system. Petersen et al. (2002) proposed that the stage 2 polymetallic sulfides formed from a combination of sulfur leached from the underlying volcanic rocks and reduced seawater sulfate, similar to that found in the majority of sea-floor hydrothermal systems. We examine alternative explanations below, especially for stage 2 mineralization.

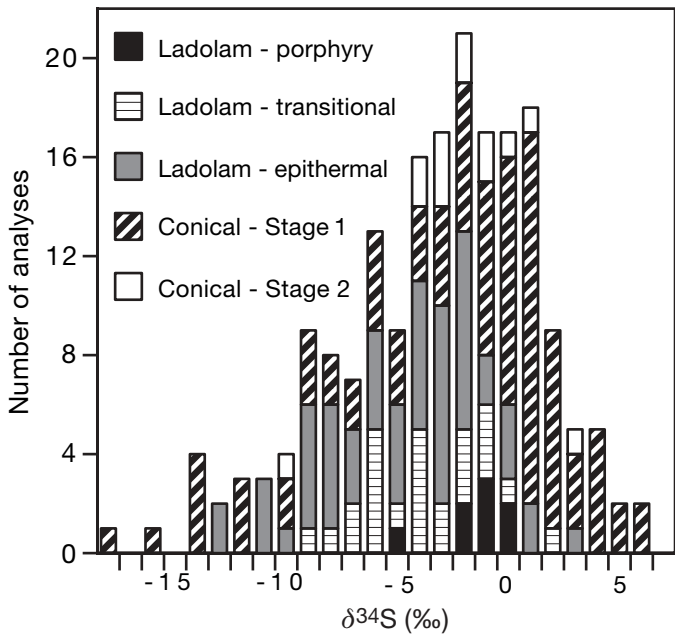

FIG. 7. Histogram comparing sulfide δ^{34}S values for the different mineralization styles at Ladolam and the mineralized stages at Conical seamount. Data from Tables 2 and 4, Müller et al. (2002a), and Carman (2003).

In order to explain the variation of δ^{34}S values at Conical seamount the potential sources of sulfur and the depositional processes at the time of mineralization need to be evaluated. The temperatures of formation were <310°C for stage 2 and <100°C for stage 3 at Conical seamount, whereas no temperature estimate was given for stage 1 (Petersen et al., 2002). We interpret that the sulfide, sulfosalt, alteration mineralogy, and temperature-solubility relationships for base and precious metals of stages 1 and 2 mineralization indicate a temperature range of between 300° to 200°C. Sulfides precipitating from inorganically reduced seawater sulfate (sulfate in the present ocean is 21.0 ± 0.2‰; Rees et al., 1978) at temperatures between 300° and 200° would have δ^{34}S values

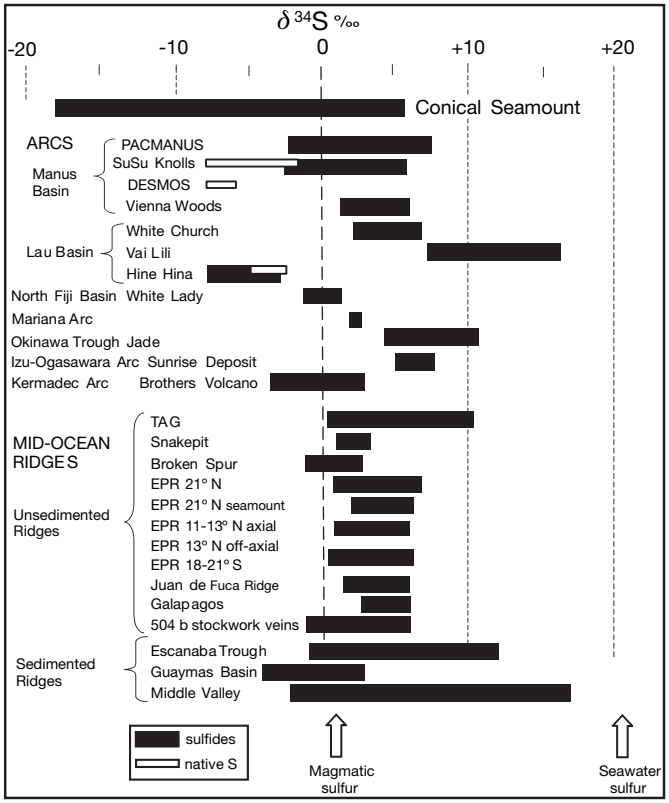

FIG. 8. Comparison of $\delta^{34}S$ values for hydrothermal sites on midocean ridges and arc environments on the modern sea floor. Modified from Gemmell and Sharpe (1998) with additional data from Gemmell et al. (1999), Goodfellow et al. (1999), Iizasa et al. (1999), and de Ronde et al. (2000).

from –4 to +21 per mil, depending on the amount of reduction and extent of equilibrium (Ohmoto and Rye, 1979). The majority of $\delta^{34}S$ values for stage 1 and 2 sulfide minerals at Conical seamount (–17 to +6‰) are significantly lower than the predicted values, indicating that reduced seawater sulfate was not the primary source of sulfur.

Petersen et al. (2002) suggested that leaching of volcanic rock sulfur was a major source of sulfur in stage 2 mineralization. The average $\delta^{34}S$ value for total sulfur (sulfide and sulfate) in midocean ridge basalt is near 0 per mil and andesites in island-arc environments have $\delta^{34}S_{total}$ values between 5 and 7 per mil (Ueda and Sakai, 1984; Woodhead et al., 1987). Although $\delta^{34}S_{total}$ values are not available for the Conical seamount alkali basalts, the isotopic signature of the Conical seamount sulfides in stages 1 and 2 requires a source of light sulfur that cannot be explained by simple nonequilibrium mixing between SO_4 and H_2S leached from the volcanic host rocks.

Therefore, based on these factors, other sulfur sources and/or processes, such as organic reduction of seawater sulfate, evolution of light sulfur directly from magmatic volatiles, and/or boiling are required to explain the light sulfur at Conical seamount. Organically reduced seawater sulfate in marine sediments has been considered an important source of isotopically light sulfur in some sea-floor hydrothermal systems (Shanks et al., 1995). The maximum temperature estimated for the production of organically reduced seawater sulfate is <120°C (Canfield, 2001). Petersen et al. (2002) suggested that bacteriogenic sulfate reduction might be involved in the formation of the framboidal pyrite, due to their low $\delta^{34}S$ values (Table 3). Hydrothermal sulfides in veins, veinlets, and disseminations with alteration in stages 1 and 2 throughout all the mineralized zones, also have very low $\delta^{34}S$ values, some lower than the framboidal pyrite (Table 2). Therefore, at temperatures between 300° and 200°C organically reduced seawater sulfate was not a significant source of sulfur in sulfide minerals from stages 1 and 2 mineralization at Conical seamount.

Our new data suggest that there was a more significant role for magmatic sulfur and boiling throughout the paragenesis than was previously recognized and that the negative sulfur isotope values in framboidal pyrite reported by Petersen et al.

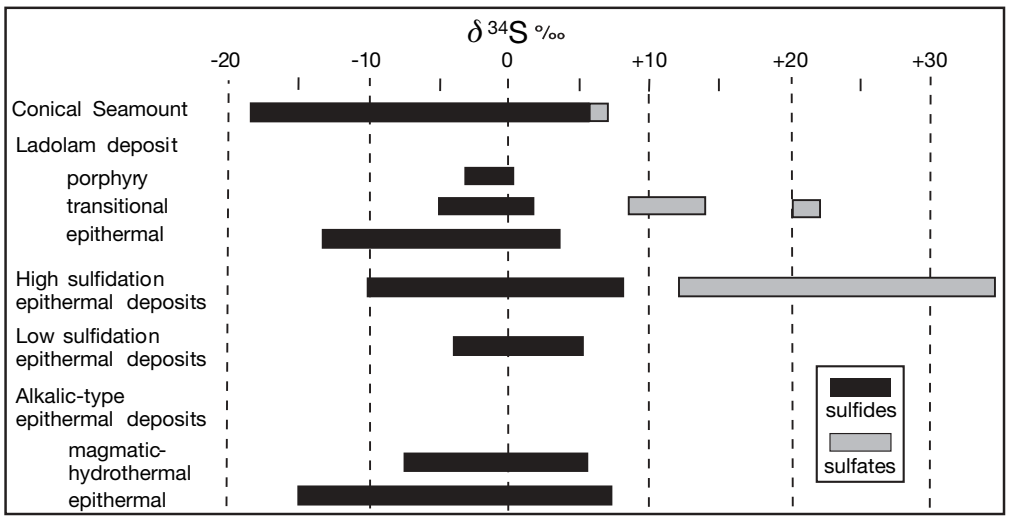

FIG. 9. Comparison of $\delta^{34}S$ values from Conical seamount and the Ladolam deposit with high-sulfidation epithermal deposits (Arribas, 1995), low-sulfidation epithermal deposits (Field and Fifarek, 1985), and the alkalic subtype of low-sulfidation epithermal deposits (Richards, 1995).

(2002) probably reflect the same strong magmatic sulfur contribution that is evident in the main stage 1 mineralization. At magmatic temperatures the dominant sulfur species is SO_2 (Sakai et al., 1984; Wallace and Carmichael, 1992), whereas as the magmatic volatiles cool below 400°C, magmatic SO_2 will disproportionate to H_2S and H_2SO_4. This process will enrich ^{32}S in the sulfide and ^{34}S in the sulfate (Ohmoto and Rye, 1979; Ohmoto and Lasaga, 1982). Sulfides precipitated from this sulfur will have $\delta^{34}S$ values <0 per mil, and coexisting sulfate minerals will have $\delta^{34}S$ values >0 per mil, although substantially lower than seawater sulfate (Herzig et al., 1998a). The $\delta^{34}S$ values for alunite (6–8‰) formed with pyrite in stage 1 at Conical seamount are markedly lower than present seawater, indicating that the sulfur in alunite was derived from magamatic volatiles.

McKibben and Eldridge (1990) determined that boiling of a hydrothermal fluid, accompanied by separation of a volatile phase, caused radical variation in the isotopic composition of sulfides. They concluded that boiling involves the loss of aqueous H_2 and H_2S into the vapor phase that causes an increase in the oxidation state of the residual liquid, leading to significant fractionation of sulfur isotopes. This fractionation can cause rapid shifts from positive to negative $\delta^{34}S$ values of sulfides that are highly variable at the grain scale, with isotopic heterogeneity in individual samples (McKibben and Eldridge, 1990). Individual samples at Conical seamount have $\delta^{34}S$ values that vary by as much as 7 per mil (Table 2). In adjacent stage 1, disseminated pyrite grains in sample 40GTVA-2 range over 4 per mil, and in sample 53GTVA-2A adjacent stage 2 sulfide grains have $\delta^{34}S$ values exceeding a range of 7 per mil. There is a wide range of $\delta^{34}S$ values within individual pyrite veins. For example sample 14-GTVA-3 has a range of over 6 per mil across the vein (Table 2). Therefore, we suggest the large variation of $\delta^{34}S$ values within pyrite is caused by boiling of the hydrothermal fluid. However, as hydrothermal fluids are not presently venting at Conical seamount there is no direct visual evidence of boiling, and no fluid inclusion investigation has been undertaken to evaluate evidence for boiling, due to the very fine grained nature of the material.

In summary, we interpret the range of $\delta^{34}S$ values in the polymetallic and pyritic stockwork mineralization (stages 1 and 2) at Conical seamount in the following way. Although the framboidal pyrite analyzed by Petersen et al. (2002) may have had an organically reduced sulfur component, we suggest that organically reduced seawater sulfate did not play a significant role in the overall sulfur budget of Conical seamount. Rather, the dominant process that produced the low $\delta^{34}S$ values in both the stage 1 and 2 sulfides was the disproportionation of magmatic SO_2. The $\delta^{34}S$ values for the sulfides (–17.5 to +6.1‰, mean = –1.9‰, this study) are generally lower than the initial $\delta^{34}S$ of SO_2 (near 0‰) and values for the associated alunite (6.4–7.5‰, Petersen et al., 2002) are higher than the starting composition but lower than coeval seawater (21‰). The presence of platy alunite, associated kaolinite, aluminum phosphate minerals, and other clay minerals in stage 1 mineralization (Herzig et al., 1998b, c, 1999; Petersen et al., 2002) supports the interpretation that magmatic fluids have contributed to the hydrothermal system at Conical seamount. The mixing of magmatic fluids with inorganically reduced seawater sulfate within Conical seamount may have produced some of the higher $\delta^{34}S$ sulfide values in stage 2 and 3 sulfides. The observed alteration (illite, montmorillonite group clays, chlorite, and adularia with minor calcite) with stage 2 mineralization (Petersen et al., 2002) suggests that interaction with seawater may have neutralized the acidity of the magmatic fluid, causing a near-neutral pH alteration assemblage to form. Boiling may have caused the large variations of $\delta^{34}S$ values within individual samples and could have been an important process in the deposition of sulfides at Conical seamount.

Ladolam deposit, Lihir Island

The magmatic-hydrothermal history at Ladolam, together with the island setting, led Carman (2003) to postulate a complex multicomponent source for the hydrothermal fluids during evolution of the deposit. Based on fluid inclusion and stable isotope evidence, Carman (2003) concluded that the stage I porphyry-style mineralization ($\delta^{34}S$ of pyrite = –1.4 to +2.2‰) was of magmatic origin. Stage II veins and breccias precipitated between 300° and 200°C, with 5 to 10 wt percent NaCl equiv due to mixing of the magmatic fluid with dilute ground water. Carman (2003) suggested that $\delta^{34}S$ values of pyrite (–7 to +2‰) and deep anhydrite (13‰) indicated a magmatic source, with no evidence of seawater input. The stage III low-sulfidation epithermal mineralization is interpreted to form from an initial magmatic brine at 230°C with 5 ± 0.5 wt percent NaCl equiv that mixed with dilute meteoric ground water to produce a hydrothermal fluid at 170° ± 20°C and near 0 wt percent NaCl equiv. Late-stage silicic breccia ores were deposited at temperatures below 200°C as reduced fluids mixed with oxidized acid-sulfate waters of low salinity beneath an advanced argillic cap (Carman, 2003).

Our data support the conclusion by Carman (2003) that the overall light sulfur and large range of $\delta^{34}S$ values at Ladolam were initially due to magmatic fluids escaping from the crystallizing magma. It is likely that during the catastrophic collapse of a portion of the Luise volcano and unroofing of the hydrothermal system (Carman, 2003), magmatic fluids were released, likely boiled due to the rapid pressure release, and mixed with dilute ground water. These processes led to lower $\delta^{34}S$ values in the stage II transitional and stage III epithermal styles of mineralization.

New sulfur isotope data on anhydrite show that there could be two populations of $\delta^{34}S$ values, one between 8 and 14 per mil and one between 20 and 22 per mil (Fig. 6B). The high $\delta^{34}S$ values raise the possibility of the interaction with seawater, previously discounted, with magmatic fluids and ground water. The lower anhydrite $\delta^{34}S$ values are likely due to the disproportionation of magmatic SO_2 leading to enrichment of ^{34}S in the sulfate but $\delta^{34}S$ values less than coeval seawater. Two anhydrite samples with $\delta^{34}S$ values of 8.6 and 11.1 per mil (Muller et al., 2002a) have reported $^{87/86}Sr$ isotope values of 0.7040, suggesting a magmatic Sr source (Muller et al., 2002b). The higher anhydrite $\delta^{34}S$ values are the same as coeval seawater sulfate and indicate that mixing with seawater did occur at Ladolam, although the amount and extent of this mixing is unknown. There are no published Sr isotope data for the anhydrite with the higher $\delta^{34}S$ values to confirm the seawater signature. The most reasonable interpretation of the present data is that the range of sulfide and sulfate $\delta^{34}S$ values

at Ladolam is due to the complex interaction of magmatic hydrothermal fluids, meteoric water, and seawater.

The fumaroles depositing native sulfur and offshore hydrothermal vents forming pyrite have the same $\delta^{34}S$ values as the Ladolam epithermal mineralization, indicating that similar fluids are still reaching the floor of the Luise caldera. Carman (2003) interpreted that the active hydrothermal system within the Luise caldera is a remnant of the Ladolam ore-forming system.

Conclusions

The discovery of Conical seamount is a unique opportunity to examine ore-forming processes in a submarine environment, which have a number of mineralogical, chemical, and textural characteristics in common with some subaerial epithermal systems. Conical seamount has the lowest, hydrothermal sulfide (i.e., nondiagenetic) $\delta^{34}S$ values (–17.5 to +6.1‰) measured to date from modern sea-floor hydrothermal systems. A model by Petersen et al. (2002) for the Conical seamount hydrothermal system suggested a contribution of magmatic volatiles in the earliest stages of mineralization (stage 1), followed by a combination of sulfur leached from the underlying volcanic rocks and reduced seawater sulfate during the main base and precious metal precipitating event (stage 2). New sulfur isotope data suggest a significant input of magmatic volatiles, and possibly boiling, throughout both stage 1 and 2 mineralization. Pyrite samples from the Ladolam gold deposit have a similar range of sulfur isotope values (–12.9 to +3.6‰) as Conical seamount. The range of sulfide and sulfate $\delta^{34}S$ values at Ladolam is interpreted to be due to the complex interaction of magmatic hydrothermal fluids, meteoric ground water, and seawater. Active fumaroles depositing native sulfur and offshore hydrothermal vents forming pyrite have the same $\delta^{34}S$ values as the Ladolam epithermal mineralization, indicating that fluids similar to those that formed the gold deposit are still reaching the floor of the Luise caldera. Sulfur isotope data at both Conical seamount and the Ladolam deposit suggest that magmatic volatiles have contributed a significant amount of sulfur to both these gold-rich hydrothermal systems.

Acknowledgments

Principal funding for the SO-133 EDISON II cruise was provided by the German Ministry for Education and Research (BMBF grant 03G0133A to Peter Herzig). We thank Master Andresen and the officers and crew of the R/V SONNE for their expert assistance and cooperation during research activities around Lihir Island. Mark Hannington is acknowledged for providing unpublished sulfur isotope data from the Ladolam deposit and environment. JBG and RS appreciate the ARC grant obtained by Ross Large for development of the Central Science Laboratory stable isotope facilities at the University of Tasmania and the Australian Research Council's Special Research Centres Program. Sulfur isotope analyses were completed with the help of Mike Power, Sr., and Christine Cook of the Central Science Laboratory, University of Tasmania. IRJ acknowledges project support from the Mineral Resources Division of the Geological Survey of Canada. Reviews by Jeremy Richards, Minoru Kusakabe, Cornel de Ronde, Jeff Hedenquist, and Mark Hannington have significantly improved early versions of this paper.

May 30, 2002; September 16, 2004

REFERENCES

Arribas, Jr., A., 1995, Characteristics of high-sulfidation epithermal deposits, and their relation to magmatic fluid: Mineralogical Association of Canada Short Course Series, v. 23, p. 419–454.

Canfield, D.E., 2001, Biogeochemistry of sulfur isotopes: Reviews in Mineralogy and Geochemistry, v. 43, p. 607–636.

Carman, G.G., 1994, Genesis of the Ladolam gold deposit, Lihir Island, Papua New Guinea: Unpublished Ph.D. thesis, Clayton, Victoria, Australia, Monash University, 300 p.

——2003, Geology, mineralization and hydrothermal evolution of the Ladolam gold deposit, Lihir Island, Papua New Guinea: Society of Economic Geologists Special Publication 10, p. 247–284.

Cooke, D.R., and Simmons, S.F., 2000, Characteristics and genesis of epithermal gold deposits: Reviews in Economic Geology, v. 13, p. 221–244.

Corbett, G.J., and Leach, T.M., 1998, Southwest Pacific Rim gold-copper systems: Structure, alteration and mineralization: Society of Economic Geologists Special Publication 6, 237 p.

Davies, R.M., and Ballantyne, G.H., 1987, Geology of the Ladolam gold deposit; Lihir Island, Papua New Guinea: Australian Institute of Mining and Metallurgy, Pacific Rim Congress 87, Gold Coast, Australia, August 26-29, 1987, Proceedings, p. 943–949.

de Ronde, C.E.J., 1995, Fluid chemistry and isotope characteristics of seafloor hydrothermal systems and associated VMS deposits: Potential for magmatic contributions: Mineralogical Association of Canada Short Course Series, v. 23, p. 479–509.

de Ronde, C.E.J., Hannington, M., Stoffers, P., Wright, I., Gennerich, H.H., Browne, P., and Herzig, P., 2000, Massive sulfiude mineralisation associated with a frontal arc volcano: Brothers hydrothermal system, southern Kermadec arc, New Zealand [abs.]: Hobart, Tasmania, Australia, Centre for Ore Deposit Research Special Publication 3, p. 37–38.

Exon, N.F., Stewart, W.D., Sandy, M.J., and Tiffin, D.L., 1986, Geology and offshore petroleum prospects of the eastern New Ireland basin, northeastern Papua New Guinea: Bureau of Mineral Resources Journal of Australian Geology and Geophysics 10, p. 39–51.

Field, C.W., and Fifarek, R.H., 1985, Light stable isotope systematics in epithermal systems: Reviews in Economic Geology, v. 2, p. 99–128.

Gamo, T., Okamura, K., Charlou, J., Urabe, T., Auzende, J., Ishibashi, J., Shitashima, K., Chiba, H., Binns, R.A., Gena, K., Henry, K., Matsubayashi, O., Moss, R., Nagaya, Y., Naka, J., and Ruellan, E., 1997, Acidic and sulfate-rich hydrothermal fluids from the Manus back-arc basin, Papua New Guinea: Geology, v. 25, p. 139–142.

Gemmell, J.B., and Sharpe, R., 1998, Detailed sulfur isotope investigation of the TAG hydrothermal mound and stockwork zone, 26°N, Mid-Atlantic Ridge: Proceedings of the Ocean Drilling Program, Scientific Results, v. 158, p. 71–84.

Gemmell, J.B., Binns, R.A., and Parr, J.,M., 1999, Submarine, high sulfidation alteration within DESMOS caldera, Manus basin, PNG, *in* C.J. Stanley et al., eds, Mineral deposits: Processes to processing, v.1, Proceedings of the 5th biennial SGA meeting and the 10th quadrennial IAGOD symposium: London, Balkema, p. 503–506.

Goodfellow, W.D., and Franklin, J.M., 1993, Geology, mineralogy, and chemistry of sediment-hosted clastic massive sulfide in shallow cores, Middle Valley, Northern Juan de Fuca Ridge: Economic Geology, v. 88, p. 2037–2068.

Goodfellow, W.D., Zierenberg, R.A, and the ODP Leg 169 Shipboard Science party, 1999, Genesis of massive sulfide deposits at sediment-covered spreading centers: Reviews in Economic Geology, v. 8, p. 297–324.

Hannington, M.D., 1997, The porphyry-epithermal-VMS transition: Lessons from the Iskut River area, British Columbia, and modern island arcs: Society of Economic Geologists Newsletter 29, p. 12–13.

Hannington, M., Poulsen, H., Thompson, J., and Sillitoe, R., 1999, Volcanogenic gold and epithermal-style mineralization in the VMS environment: Reviews in Economic Geology, v. 8, p. 325–356.

Hedenquist, J.W., and Lowenstern, J.B., 1994, The role of magmas in the formation of hydrothermal ore deposits: Nature, v. 370, p. 519–527.

Herzig, P.M., and Hannington, M.D., 1995a, Polymetallic massive sulfides at the modern seafloor—a review: Ore Geology Reviews, v. 10, p. 95–115.

——1995b, Hydrothermal activity, vent fauna, and submarine gold mineralization at alkaline fore-arc seamounts near Lihir Island, Papua New Guinea: Australian Institute of Mining and Metallurgy, Pacific Rim Congress 1995, Melbourne, Australia, Proceedings, p. 279–284,

Herzig, P., Hannington, M., McInnes, B, Stoffers, P., Villinger, H., Seifert, R., Binns, R., and Liebe, T., 1994, Submarine volcanism and hydrothermal venting studied in Papua New Guinea: EOS Transactions, v. 75, no. 44, p. 513–616.

Herzig, P.M., Hannington, M.D., and Arribas, Jr., A., 1998a, Sulfur isotope composition of hydrothermal precipitates from the Lau back-arc: Implications for magmatic contributions to seafloor hydrothermal systems: Mineralium Deposita, v. 33, p. 226–237.

Herzig, P., Hannington, M., Stoffers, P., and Shipboard Party, 1998b, Volcanism, hydrothermal processes and biological communities at shallow submarine volcanoes of the New Ireland fore-arc, Papua New Guinea: Freiberg, Germany, Freiberg University, Cruise Report Sonne-133, 146 p.

——1998c, Petrology, gold mineralization, and biological communities at shallow submarine volcanoes of the New Ireland fore-arc (Papua New Guinea): Preliminary results of R/V Sonne cruise SO-133: InterRidge News, v. 7(2), p. 34–38.

Herzig, P.M., Petersen, S. and Hannington, M.D., 1999, Epithermal-type gold mineralization at Conical seamount: A shallow submarine volcano south of Lihir Island, Papua New Guinea, *in* C.J. Stanley et al., eds, Mineral deposits: Processes to processing, v. 1, Proceedings of the 5th biennial SGA meeting and the 10th Quadrennial IAGOD symposium: London, Balkema, p. 527–530.

Huston, D.L., Power, M., Gemmell, J.B., and Large, R., 1995, Design, calibration and geologic application of the first operational Australian laser ablation sulphur isotope microprobe: Australian Journal of Earth Sciences, v. 42, p 549–555.

Iizasa, K., Fiske, R.S., Ishizuka, O., Yuasa, M., Hashimoto, J., Ishibashi, J., Naka, J., Horii, Y., Fujiwara, Y., Imai, A., and Koyama, S., 1999, A kurokotype polymetallic sulfide deposit in a submarine silicic caldera: Science, v. 283, p. 975–977.

Jensen, E.P., and Barton, M.D., 2000, Gold deposits related to alkaline magmatism: Reviews in Economic Geology, v. 13, p. 279–314.

Kennedy, A.K., Hart, S.R., and Frey, F.A., 1990, Composition and isotopic constraints on the petrogenesis of alkaline arc lavas: Lihir Island, Papua New Guinea: Journal of Geophysical Research, v. 95, p. 6929–6942.

McInnes, B.I.A., 1992, A glimpse of ephemeral subduction zone processes from Simberi Island, Papua New Guinea: Unpublished Ph.D. thesis, Ottawa, Canada, University of Ottawa, 235 p.

McInnes, B.I.A., and Cameron, E.M., 1994, Carbonated, alkaline metasomatic melts from a sub-arc environment: Mantle wedge samples from the Tabar-Lihir-Tanga-Feni arc, Papua New Guinea: Earth and Planetary Science Letters, v. 122, p. 125–141.

McInnes, B.I.A., McBride, J.S., Evans, N.J., Lambert, D.D., and Andrew, A.S., 1999, Osmium isotope constraints on metal recycling in subduction zones: Science, v. 286, p. 512–516.

McInnes, B.I.A., Gregoire, M., Binns, R.A., Herzig, P.M., and Hannington, M.D., 2001, Hydrous metasomatism of oceanic sub-arc mantle, Lihir, Papua New Guinea: Petrology and geochemistry of fluid-metasomatized mantle wedge xenoliths: Earth and Planetary Science Letters, v. 188, p. 169–183.

McKibben, M.A., and Eldridge, C.S., 1990, Radical sulfur isotope zonation of pyrite accompanying boiling and epithermal gold deposition: A SHRIMP study of the Valles caldera, New Mexico: Economic Geology, v. 85, p. 1917–1925.

Moyle, A.J., Doyle, B.J., Hoogvliet, H., and Ware, A.R., 1990, Ladolam gold deposit, Lihir Island: Australian Institute of Mining and Metallurgy Monograph 14, p. 1793–1805.

Müller, D., Franz, L., Herzig, P.M., and Hunt, S., 2001, Potassic rocks from the vicinity of epithermal gold mineralization, Lihir Island, Papua New Guinea: Lithos, v. 57, p. 163–186.

Müller, D., Herzig, P.M., Scholten, J.C., and Hunt, S., 2002a, Ladolam gold deposit, Lihir Island, Papua New Guinea: Gold mineralization hosted by alkaline rocks: Society of Economic Geologists Special Publication 9, p. 367–382.

Müller, D., Kaminski, K., Uhlig, S., Graupner, T., Herzig, P.M., and Hunt, S., 2002b, The transition from porphyry- to epithermal-style gold mineralization at Ladolam, Lihir Island, Papua New Guinea: A reconnaissance study: Mineralium Deposita, v. 37, p. 61–74.

Ohmoto, H., 1986, Stable isotope geochemistry of ore deposits: Reviews in Mineralogy, v. 16, p. 491–560.

Ohmoto, H., and Lasaga, A.C., 1982, Kinetics of reactions between aqueous sulfates and sulfides in hydrothermal systems: Geochimica et Cosmochimica Acta., v. 46, p. 1727–1745.

Ohmoto H., and Rye, R.O., 1979, Isotopes of sulphur and carbon, *in* Barnes, H.L., ed., Geochemistry of hydrothermal ore deposits: New York, Wiley and Sons, p. 509–567.

Petersen, S., Herzig, P.M., Hannington, M.D., and Jonasson, I.R., 2002, Submarine gold mineralization near Lihir Island, New Ireland fore-arc, Papua New Guinea: Economic Geology, v. 97, p. 1795–1813.

Pichler, T., Giggenbach, W.F., McInnes, B.I.A., Buhl, D., and Duck, B., 1999, Fe sulfide formation due to seawater-gas-sediment interaction in a shallow-water hydrothermal system at Lihir Island, Papua New Guinea: Economic Geology, v. 94, p. 281–288.

Rees, C.E., Jenkins, W.J., and Monster, J., 1978. The sulfur-isotope geochemistry of ocean water sulfate: Geochimica et Cosmochimica Acta, v. 42, p. 377–382.

Richards, J.P., 1995, Alkalic-type epithermal gold deposits—a review: Mineralogical Association of Canada Short Course Series, v. 23, p. 367–400.

Robinson, B.W., and Kusakabe, M., 1975, Quantitative preparation of SO_2 for $^{34}S/^{32}S$ analyses from sulfide by combustion with cuprous oxide: Analytical Chemistry, v. 7, p. 1179–1181.

Sakai, H., Des Marais, D.J., Ueda, A., and Moore, J.G., 1984, Concentrations and isotope ratios of carbon, nitrogen and sulfur in ocean-floor basalts: Geochimica et Cosmochimica Acta, v. 48, p. 2433–2441.

Sangster, D.F., 1968, Relative sulfur-isotope abundances of ancient seas and stratabound sulfide deposits: Geological Association of Canada Proceedings, v. 17, p. 79–91.

Shanks, W.C., III, Bischoff, J.L., and Rosenbauer, R.J., 1981, Seawater sulfate reduction and sulfur-isotope fractionation in basaltic systems: Interactions of seawater with fayalite and magnetite at 200–350°C: Geochimica et Cosmochimica Acta, v. 45, p. 1977–1995.

Shanks, W.C., III, Bohlke, J.K., and Seal, R.R., III, 1995, Stable isotopes in mid-ocean ridge hydrothermal systems: Interactions between fluids, minerals, and organisms: Geophysical Monograph 91, p. 194–221.

Shipboard Scientific Party, 2002, Leg 193 summary: Proceedings of the Ocean Drilling Program Initial Reports, v. 193, p. 1–84.

Sillitoe, R.H., Hannington, M.D., and Thompson, J.F.T., 1996, High-sulfidation deposits in the volcanogenic massive sulfide environment: Economic Geology, v. 91, p. 204–212.

Solomon, M., Eastoe, C.J., Walshe, J.L., and Green, G.R., 1988, Mineral deposits and sulfur-isotope abundances in the Mount Read Volcanics between Que River and Mount Darwin, Tasmania: Economic Geology, v. 83, p. 1307–1328.

Stewart, W.D., and Sandy, M.J., 1988, Geology of New Ireland and Djaul Islands, northeastern Papua New Guinea: Circum-Pacific Council for Energy and Mineral Resources, Earth Science Series 9, p. 13–30.

Taylor, B.E., 1987, Stable isotope geochemistry of ore-forming fluids: Mineralogical Association of Canada Short Course Handbook, v. 13, p. 337–445.

Ueda, A., and Sakai, H., 1984, Sulfur isotope study of Quaternary volcanic rocks from the Japanese islands arc: Geochimica et Cosmochimica Acta, v. 48, p 1837–1848.

Wallace, D.A., Johnson, R.W., Chappell, B.W., Arculus, R.J., Perfit, M.R., and Crick, I.H., 1983, Cainozoic volcanism of the Tabar, Lihir, Tanga and Feni Islands, Papua New Guinea: Geology, whole-rock analyses, and rock-forming mineral compositions: Bureau of Mineral Resources, Geology, and Geophysics Australia Report 243 (microfiche).

Wallace, P., and Carmichael, I.S.E., 1992, Sulfur in basaltic magmas: Geochimica et Cosmochimica Acta, v. 56, p. 1863–1847.

Woodhead, J.D., Harmon, R.S., and Fraser, D.G., 1987, O, S, Sr and Pb isotope variations in volcanic rocks from the northern Mariana Islands: Implications for crustal recycling in intra-oceanic arcs: Earth and Planetary Science Letters, v. 83, p. 39–52.

Yang, K., and Scott, S.D., 1996, Possible contribution of a metal-rich magmatic fluid to a sea-floor hydrothermal system: Nature, v. 383, p. 420–423.